Finite amplitude electroconvection induced by strong unipolar injection between two coaxial cylinders

Jian Wu[a], Pedro A. Vázquez[b], Philippe Traoré[a1], Alberto T. Pérez[c]

[a] Institut PPRIME, Département Fluide-Thermique-Combustion, Boulevard Pierre et Marie Curie, BP 30179, 86962 Futuroscope-Chasseneuil, France

[b] Departamento de Física Aplicada III, Universidad de Sevilla, ESI, Camino de los Descubrimientos s/n, 41092 Sevilla, Spain

[c] Departamento de Electrónica y Electromagnetismo, Universidad de Sevilla, Facultad de Física, Avenida Reina Mercedes s/n, 41012 Sevilla, Spain

Abstract

We perform a theoretical and numerical study of the Coulomb-driven electroconvection flow of a dielectric liquid between two coaxial cylinders. The specific case where the inner to outer diameter ratio is 0.5 is analyzed. A strong unipolar injection of ions either from the inner or outer cylinder is considered to introduce free charger carriers into the system. A finite volume method is used to solve all governing equations including Navier-Stokes equations and a simplified set of Maxwell's equations. The flow is characterized by a subcritical bifurcation in the finite amplitude regime. A linear stability criterion and a nonlinear one that correspond to the onset and stop of the flow motion, respectively, are linked with a hysteresis loop. In addition, we also explore the behavior of the system for higher values of the stability parameter. For inner injection, we observe a transition between the patterns made of 7 and 8 pairs of cells, before an oscillatory regime is attained. Such a transition leads to a second finite amplitude stability criterion. A

[1]Corresponding author. E-mail address: philippe.traore@univ-poitiers.fr (P. Traoré).

simple modal analysis reveals that the competition of different modes is at the origin of this behavior. The charge density as well as velocity field distributions are provided to help understanding the bifurcation behavior.

Key words: Electroconvection; stability analysis; charge injection; numerical simulation; dielectric liquid, annular geometry.

1. INTRODUCTION

Coulomb-driven convection is a classic example of electroconvection in dielectric liquids [1]. The Coulomb force exerting on free charge carries drives the fluid into motion. For ohmic or quasi-ohmic liquids, the free charges are considered to come from a thermally induced conductivity gradient [2] or the electric field-enhanced dissociation (the Onsager Effect) [3,4]. For dielectric liquids of very low conductivity under strong electric field, the ions injected from the interface between the liquid and electrode are more relevant [5,6]. The charge injection induced convection has received a tremendous attention since four decades because it plays a fundamental role in understanding the current voltage characteristic for dielectric liquids [7,8,9,10].

Various geometries of electrodes have been considered to study electrohydrodynamics (EHD) flows [11]. Three configurations of symmetrically placed electrodes (i.e. parallel plates, concentric cylinders and spheres) are especially interesting. This is because, under the assumption of homogeneous unipolar injection, the system possesses a hydrostatic state that is potentially unstable, implying a linear instability bifurcation. Therefore the linear stability analysis approach can be used to gain a first insight of the problem by predicting the onset of the flow motion. Atten and Moreau treated the case of parallel plates [12]. They showed that the stability criterion is highly dependent on the injection strength (i.e. the amount of charges

injected into the bulk) and independent of the dimensionless mobility parameter. The experimental results reported in [13,14] partially verified the prediction of the stability analysis. The cases of concentric cylinders and spheres were considered later in [15,16,17,18] and [19], respectively. These analyses clearly showed that, for the latter two configurations, two factors including the ratio between the radii of cylinders or spheres and the injection direction (from the inner or outer electrode) make the problem more intricate than the planar geometry. Later, Pontiga and Castellanos extended the study to dielectric liquids with impurities by simultaneously considering the ion injection and electric field enhanced dissociation in the cylindrical geometry [20].

Another feature of the injection induced electroconvection in the planar configuration lies in its subcritical bifurcation [21,22]. Associated to this bifurcation there exists a nonlinear stability criterion in the finite amplitude regime corresponding to the stop of the flow motion. This subcritical bifurcation is essentially related to the two transport mechanisms for ions, i.e. drift by the electric field and convection by the velocity field of fluid. The competition between the two mechanisms leads to the formation of regions free of charges [22,23]. In the planar geometry, Atten and Lacroix performed a weakly nonlinear stability analysis and determined the nonlinear criteria for various injection strengths [22]. The nonlinear phenomenon was also confirmed by the experimental results in the space-charge-limited (SCL) regime [24]. However, as far as we know, no attempt has been conducted for the investigation of the nonlinear instability of electroconvection in the annular geometry.

In recent years, several numerical simulations have been successfully conducted to study the electroconvection in the planar configuration [25,26,27,28,29,30,31,32,33]. A key component in designing the numerical algorithm for Coulomb-driven flows is the method employed to solve the

charge transport equation. Since the molecular diffusion mechanism is often neglected, the charge density equation is essentially hyperbolic, which requires *special* treatment to obtain accurate and oscillation-free solutions [34,35]. Several alternatives such as the particle-in-cell (PIC), flux corrected transport (FCT), method of Characteristic (MoC), discontinuous Galerkin (DG) and total variation diminishing (TVD) schemes have been used to compute the charge density distribution; see the review papers [11,36]. Recalling the early failures with low-order schemes (for example, [23,37]), the success of recent algorithms is highlighted through the accurate determination of the charge-free region and the finite amplitude criterion. Very recently, Fernandes et al. performed the numerical study of the two-dimensional charge injection induced annular electrocovnvection [38]. Though a good agreement between their numerical predictions of the linear stability criteria and the ones provided by the stability analysis was shown, they did not investigate the subcritical bifurcation and did not determine the finite amplitude stability criterion. As a matter of fact, we noticed that an upwind scheme was used in [38] to solve the charge density equation. This low order scheme seriously limited the ability of their numerical solver in studying the nonlinear bifurcation.

In this paper, we extend our previous studies of electroconvection between parallel plates [29,32,33] to the annular electroconvection between two concentric cylinders. Comparing to the planar geometry, the extra interests of the cylindrical geometry include two main aspects. First, no lateral-wall effect makes the experimental set-up more realizable and the interpretation of experimental results easier [39,40,41]. Second, the cylindrical geometry represents a situation that is closer to practical applications, considering the case of electrohydrodynamically enhanced heat transfer with the forced flows in pipes (wire/cylinder) [42,43]. The first work on the annular Coulomb-driven convection was concerned with the experimental study of the heat transfer

augmentation in circular pipes [44]. Up to 1200% increase of the heat transfer rate due to the imposed electric field was observed. Another experimental set-up was developed to preliminarily characterize the annular convection [45] and its effect on heat transfer [46]. Other studies include the linear stability analysis [15,16,17,18] and a numerical simulation [38] mentioned above. We contribute to this topic by investigating the bifurcation behavior of the motion in the finite amplitude regime.

The remainder of this paper is organized as follows. In the next section the physical problem, governing equations and boundary conditions are stated. Section 3 briefly explains the numerical methods. Results and discussions are presented in Section 4. Finally a conclusion is drawn in section 5.

2. PROBLEM FORMULATION

2.1 Physical problem and governing equations

The system under consideration is a dielectric liquid layer enclosed between two concentric infinite cylinders of radius R_i and R_o respectively (Figure 1). The fluid of density ρ_0, dynamic viscosity η and permittivity ε, is assumed to be incompressible and perfectly insulating. The layer is subjected to an electrical potential difference $\Delta V = V_0 - V_1$ which will induce a radial electric field $\vec{E}$ and charge injection into the bulk from the emitter electrode. We consider the case of unipolar injection, which means that ions are injected from one electrode only. The emitter electrode can be the inner cylinder or the outer one. The complete formulation of a dielectric liquid subjected to electric field is governed by the following EHD equations [1],

$$\nabla \cdot \vec{u} = 0, \tag{1}$$

$$\rho_0\left(\frac{\partial \vec{u}}{\partial t}+(\vec{u}\cdot\nabla)\vec{u}\right)=-\nabla\tilde{p}+\eta\Delta\vec{u}+q\vec{E}, \tag{2}$$

$$\frac{\partial q}{\partial t}+\nabla\cdot\left(q\left(\vec{u}+K\vec{E}\right)-D\nabla q\right)=0, \tag{3}$$

$$\Delta V=-\frac{q}{\varepsilon}, \tag{4}$$

$$\vec{E}=-\nabla V, \tag{5}$$

The flow is considered to be two dimensional. Here $\vec{u}\equiv[u,v]$ is the fluid velocity and q is the charge density. $\tilde{p}$ denotes the modified pressure which includes the dynamic pressure and the scalar from which the electrostriction force derives [10]. As the fluid is assumed to be isothermal, the dielectric force vanishes and only the Coulomb force $q\vec{E}$ is retained. There are three distinct mechanisms for the transport of free charges: convection with the fluid velocity ($q\vec{u}$), drift under the influence of the electric field ($qK\vec{E}$, K being the ionic mobility) and the molecular diffusion ($D\nabla q$, D being the diffusion coefficient). We neglect as it is often the case the molecular diffusion [47], aiming to keep consistent with previous studies (e.g., [15,16,17]). Consequently, Eqn. (3) becomes hyperbolic. We further assume the injection to be *homogeneous* and *autonomous*, which means that the density of charge at the emitter electrode is constant in time and always equals to q_0. In other words, the injecting process is neither influenced by the electric field nor by the liquid motion.

For universality in the description of the problem it is particularly convenient to work with non-dimensional equations. We take as units the interelectrode spacing $L=(R_o-R_i)$ for length, ΔV for electrical potential, ionic velocity scale $K\Delta V/H$ for velocity, $\rho K^2\Delta V^2/H^2$ for pressure, $H^2/K\Delta V$ for time and $\varepsilon\Delta V/H^2$ for charge density, leading to the following set of dimensionless numbers:

$$T=\frac{\varepsilon\Delta V}{\rho_0\nu\ K},\qquad C=\frac{q_0L^2}{\varepsilon\Delta V},\qquad M=\frac{1}{K}\left(\frac{\varepsilon}{\rho_0}\right)^{1/2}. \tag{6}$$

The electric Rayleigh number T represents the intensity of the driving Coulomb force. The injection strength parameter C is a measure of the injection level. According to the definition in [48], the injection can be classified into three regimes: strong ($5 < C$), medium ($0.2 < C < 5$) and weak ($C < 0.2$). The dimensionless mobility parameter M is defined as the ratio of the so-called hydrodynamic mobility and the true mobility of ions. Typical values for dielectric liquids obey $M \geq 3$ [10]. In addition, the problem also depends on the geometry of the concentric annulus. We define the radius ratio $\Gamma = R_i/R_o$.

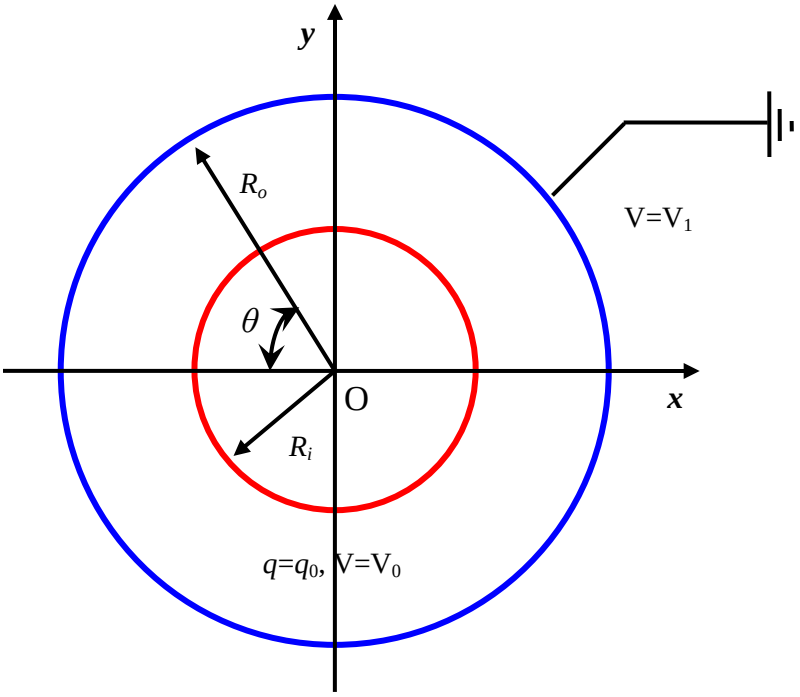

FIG. 1 Sketch of the physical domain and boundary conditions.

The resulting non-dimensional equations are therefore:

$$\nabla\cdot\overset{\omega}{u}=0, \tag{7}$$

$$\frac{\partial \varpi}{\partial t} + (\varpi \cdot \nabla)\varpi = -\nabla \tilde{p} + \frac{M^2}{T}\Delta \varpi + M^2 q\varpi, \tag{8}$$

$$\frac{\partial q}{\partial t} + \nabla \cdot \left(q\left(\varpi + \varpi\right)\right) = 0, \tag{9}$$

$$\Delta V = -q, \tag{10}$$

$$\omega = -\nabla V. \tag{11}$$

To show the strength of the flow motion, the electric Nusselt number *Ne* will be output. *Ne* is defined as the ratio of the total current I_e to the conductive current I_0, i.e. without any flow motion. In the cylindrical geometries, I_e can be calculated from $I_e = \int_0^{2\pi} \left[q\left(\varpi + \varpi\right) \cdot \varpi + \frac{\partial\left(\varpi \cdot \varpi\right)}{\partial t} \right]_{r=\text{constant}} d\theta$, $R_i \le r \le R_o$, where ω is the normal unit vector directing outward. The last part in the brackets represents the displacement current. According to the Ampère's law, I_e is independent of the radius *r*.

2.2 Boundary and initial conditions

The non-dimensional computational domain is defined by the annulus $R_i = \frac{\Gamma}{1-\Gamma} \le r \le R_o = \frac{1}{1-\Gamma}$ and $0 \le \theta \le 2\pi$. The no-slip conditions ($u = v = 0$) for velocities on electrodes are applied. The other boundary conditions read as: on the emitter cylinder, V = 1 and $q = C$; on the collecting cylinder, V = 0.

As the governing equations are time-dependent, we have to provide initial conditions. According to the purpose one could start from the zero-field for all variables, the hydrostatic state or a convective state obtained in previous simulations. The hydrostatic state means that the liquid stays at rest while ions solely move with the drift velocity, and it can be expressed as [17],

$$\vec{u}_s = [0,0],\quad q_s(r) = A_e\left[\delta\left(r^2 + B_e\right)\right]^{-1/2} \quad \text{and} \quad E_s(r) = \left(\frac{\delta A_e}{r}\right)\left[\delta\left(r^2 + B_e\right)\right]^{1/2}, \tag{12}$$

where $\delta = +1$ and -1 for the inner and outer injection, respectively. A_e and B_e are two constants depending on Γ, C and the injection direction. The implicit functions giving the coefficient A_e and B_e can be found in [17]. In the case of strong injection C=10, the values for A_e and B_e can be found in the Table I.

TABLE I. A_e and B_e coefficients in the hydrostatic solution of Eqn.(12).

Γ	0.1	0.2	0.3	0.4	0.5	0.6	0.7	0.8	0.9
Inner injection									
A_e	1.009	1.099	1.193	1.302	1.439	1.622	1.886	2.325	3.309
B_e	-0.0022	-0.050	-0.169	-0.427	-0.979	-2.224	-5.409	-15.946	-80.890
Outer injection									
A_e	0.450	0.608	0.759	0.919	1.104	1.333	1.644	2.134	3.177
B_e	-1.237	-1.566	-2.047	-2.786	-4.012	-6.268	-11.138	-25.046	-100.101

3. NUMERICAL METHODS

The whole set of partial differential equations (7) - (11) are discretized using a 2nd order in time and space finite volume method [49]. The computational domain is discretized with a structured grid consist of nonorthogonal quadrilaterals. All variables are stored at the center of each control volume, i.e. colocated arrangement. The central differencing (CD) scheme and the improved deferred correction (IDC) scheme [50] are used to compute the convective and diffusive fluxes in the Navier-Stokes equations, respectively. The 2nd order semi-implicit three time levels (I3L) scheme [49] is used for the time integration. As the fluid is assumed to be

incompressible, the velocity-pressure coupling algorithm is undertaken by the SIMPLE algorithm [51].

The solving of the equations (9)-(11) has been well detailed in [29, 52]. To prevent the development of possible oscillations in the charge density distribution, it is recommended to use non oscillating, non diffusive and bounded schemes in solving Eqn. (3) [35,53]. Total Variation Diminishing (TVD) schemes have these desirable properties [54]. In this study we have chosen the 3rd order Smooth Monotonic Algorithm for Real Transport (SMART) scheme of Gaskell & Lau [55]. The interested readers may refer to [29,52] for additional details. The improved Least-squares approach [56] is used to compute all gradients including the electric field.

4. RESULTS AND DISSCUSIONS

We consider a typical injection strength of C = 10 that has been extensively discussed in the plate-plate configuration. This strong injection regime can also been viewed as an approximation of the SCL regime, which can be achieved experimentally by using the ion-exchange membranes [13,57]. The radius ratio is fixed, Γ = 0.5, (i.e. R_i = 1.0 and R_o =2.0), while the injection can be either from the inner or the outer side. All numerical results are obtained with M = 10 unless stated otherwise.

4.1 Steady hydrostatic solutions

The validity and accuracy of our numerical solver is first checked by comparing the practicable analytical solution and the numerical one. To this end, the computation runs starting from zero-field values and without computing the fluid velocity. On figure 2 we have displayed the profiles of charge density and electric field along a radial line. Excellent agreements are obtained between our numerical solutions and the analytical ones. It is shown that both the charge density and

electric field show a dramatic variation within the region close to the emitter, which is due to the strong Coulomb repulsion between charges [23]. In addition, an even more rapid decrease is readily shown in the charge density profile of the outer injection than in the inner case.

The different distribution characteristics of the charge density induced by the inner and outer injections imply different requirements for the grid design. The use of non-uniform grids in the radial direction is desirable for better accuracy. After several grid independence tests, we finally choose a non-uniform grid with 400×150 cells (finer near the inner electrode) and a non-uniform grid with 400×175 cells (finer near the outer electrode) for the results of the inner and outer injection, respectively.

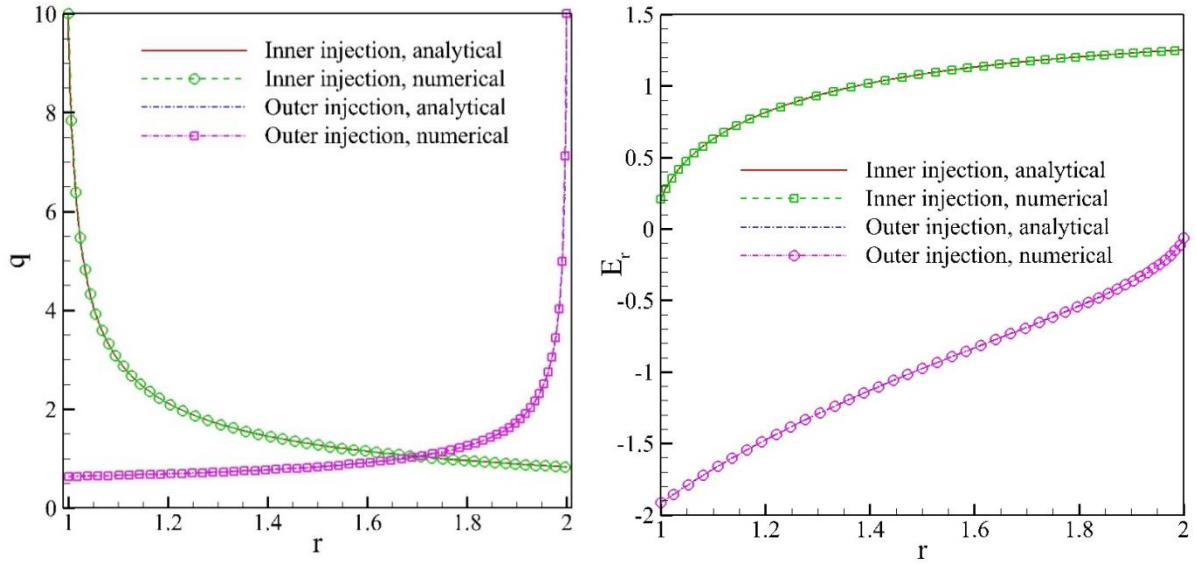

(a) (b)

FIG. 2. Comparison between the numerical and analytical solutions of the hydrostatic state, (a) charge density; (b) electric field.

4.2 Linear instability of the hydrostatic state

We alternatively consider the electroconvection induced by the charge injection from the inner or outer electrode. In [17] Agrait and Castellanos considered the complete 3D linear stability

problem. In order to compare the results from our numerical simulations with the analytical results, we have adapted their study to the 2D case with longitudinal modes. We have solved the resulting eigenvalue problem using the bvp4c function in MATLAB. This function implements a collocation method with C1 piecewise cubic polynomials [58]. For the case C = 10, Γ = 0.5 we obtain the critical values T_c = 122.84 (m_c = 7, m_c being the critical Fourier mode) for inner injection and T_c = 221.38 (m_c = 8) for outer injection. A comment must be made when comparing these results with those of Richardson in [16]. In this paper the author analyzes the inner injection case with the same configuration as us. For Γ = 0.5 and an injection parameter C_* = 10 he obtains a critical value T_c = 144.18, which seems to differ from our results. The reason of this discrepancy lies in the fact that the injection parameter C_* is defined in a different way than C. Richardson gives the expression relating these two values. It turns out that the C_* = 10 used in Richardson's paper corresponds to C = 4.342. For this value of C, our computation of the linear stability analysis gives T_c = 144.18, in perfect agreement with Richardson's result.

It is also worth mentioning that in in both cases, inner and outer injection, the critical values are higher than the values obtained for 3D instabilities [17]. In the 3D case, for inner injection it is T_c = 119.8 (2.5% of difference) and for outer injection it is T_c = 200.5 (10% of difference). The explanation for these discrepancies is the value of the critical 3D wavenumber k_c. For inner injection is k_c = 1.79, while for the outer injection is k_c = 4.33. Therefore, the inner injection case is closer to a 2D geometry, where the flow does not depend on the coordinate along the axis and k_c would be 0.

To obtain numerically the critical values T_c, we gradually increase T from zero until the onset of motion. Experimentally this would be done by continuously adjusting the applied voltage. For both injection directions, we observe that the convection only takes place when T is higher than

some critical values. Figure 3 plots the time histories of the maximum vertical velocity for several values of T higher than T_c. For all cases, there are three different stages: initially a hydrostatic one, then an exponential growth (the scale of Y-axis is logarithmic), and finally a steady convection state. At the final state, the maximum value of the radial velocity is greater than 1, and a pattern of stationary convective vortices is formed. In Figures 4 and 5 we have depicted the charge density, and the corresponding velocity field and isocontours of stream function for inner and outer injection, respectively. There are 7 and 8 pairs of counter-rotating vortices in Figures 4b and 5b. These values are consistent with the critical Fourier modes m_c [59].The exponential growth rate can be used to determine the linear stability criterion [29,31,37]; see the insets of Figure 3. The critical values for inner and outer injections are found to be 123.06 and 222.20, respectively. These values are in good agreement with the ones obtained from the linear stability analysis.

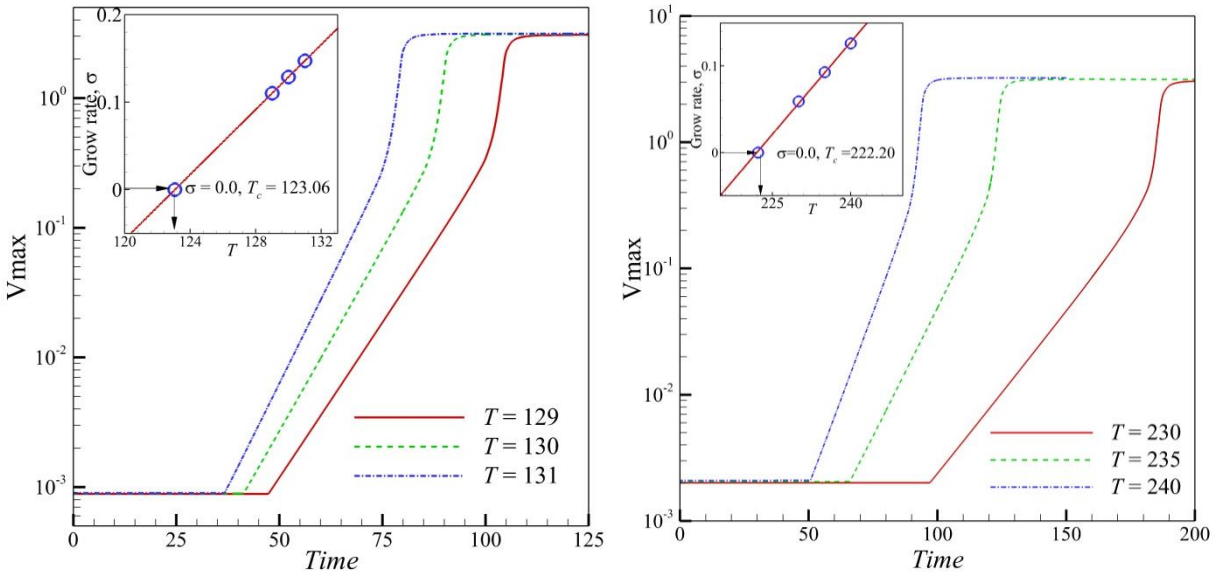

(a) (b)

FIG. 3. Temporal evolutions of the maximum vertical velocity in the logarithmic scale for (a) inner and (b) outer injection.

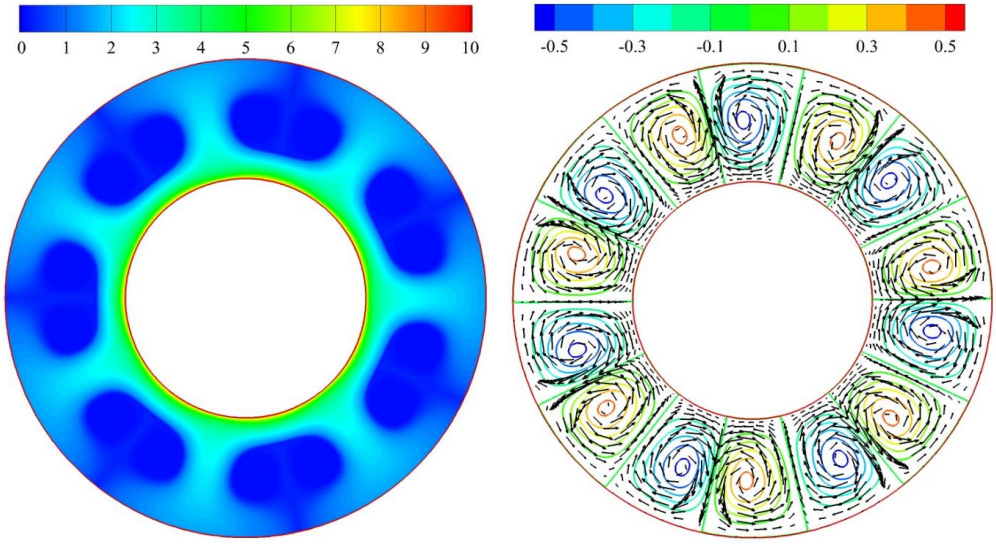

(a) (b)

FIG. 4. Distributions of (a) charge density and (b) stream function and velocity field for the inner injection with T = 131.

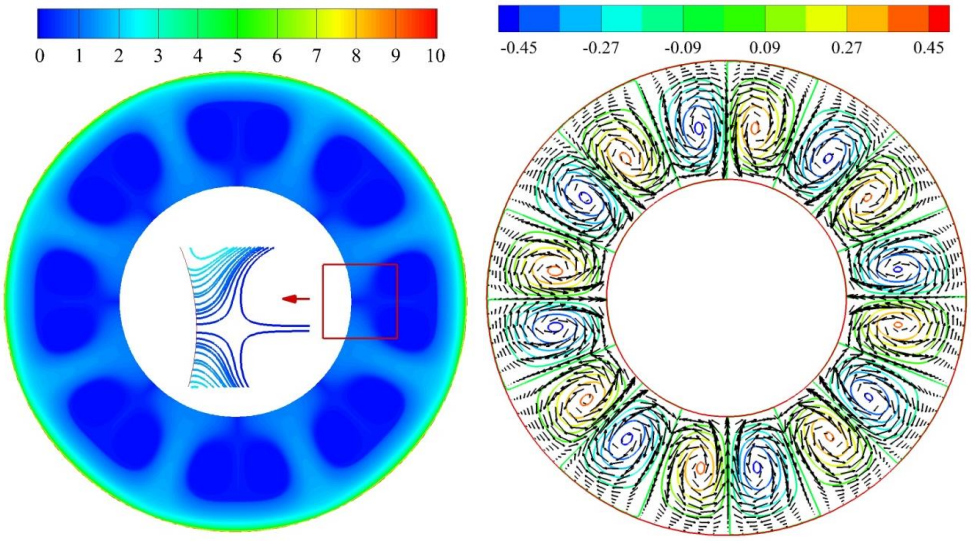

(a) (b)

FIG. 5. Distributions of (a) charge density and (b) stream function and velocity field for the inner injection with T = 260.

The charge density distributions shown in Figure 4a and 5a share strong analogy with the case of the planar configuration. For both directions, there are sharp variations in the radial direction,

especially in the region close to the emitter. In addition, we observe some central regions which are almost free of charges ($q \rightarrow 0$). These charge-free regions are very characteristic feature of Coulomb-driven convection, and they are closely related to the finite amplitude bifurcation behavior of the convection [22]. There are 7 and 8 charge-free cells in Figure 4a and 5a, same as the numbers of vortex pairs. It should be noted that each charge void region is not closed but with an opening on the collecting electrode. This opening is due to the Coulomb repulsion of charges [47], and it has already been detected numerically in the planar configuration [25,29,31].

4.3 Finite-amplitude instability of the convective state

We restart the computation from the previously obtained steady convection and gradually decrease T to determine the route of the system back to rest. It is observed that the strength of the flow motion gradually decreases with the decrease of T. At another critical value which is smaller than T_c, the motion suddenly stops. This second critical value corresponds to the suppression of the finite amplitude perturbations, and it is defined here as the nonlinear stability criterion T_{f1}. The linear and nonlinear stability criteria together with the hysteresis loop linking them fully define the subcritical bifurcation of the annular Coulomb-driven convection. The subcritical convection with the planar geometry has been well explained analytically [22,60], observed numerically [25,27,29,31,32] and confirmed experimentally [13]. In the present study, the nonlinear bifurcation with the annular electroconvection has been determined numerically.

On Figure 6 we have plotted profiles of the radial velocity V_r along the mid-section circle $r = (R_i+R_o)/2$. Figure 7 shows the change of the charge-free region represented by the area of $q<0.05$. The isoline of $q = 0.05$ represents the separatrix between the region filled with charges and the region without charges.

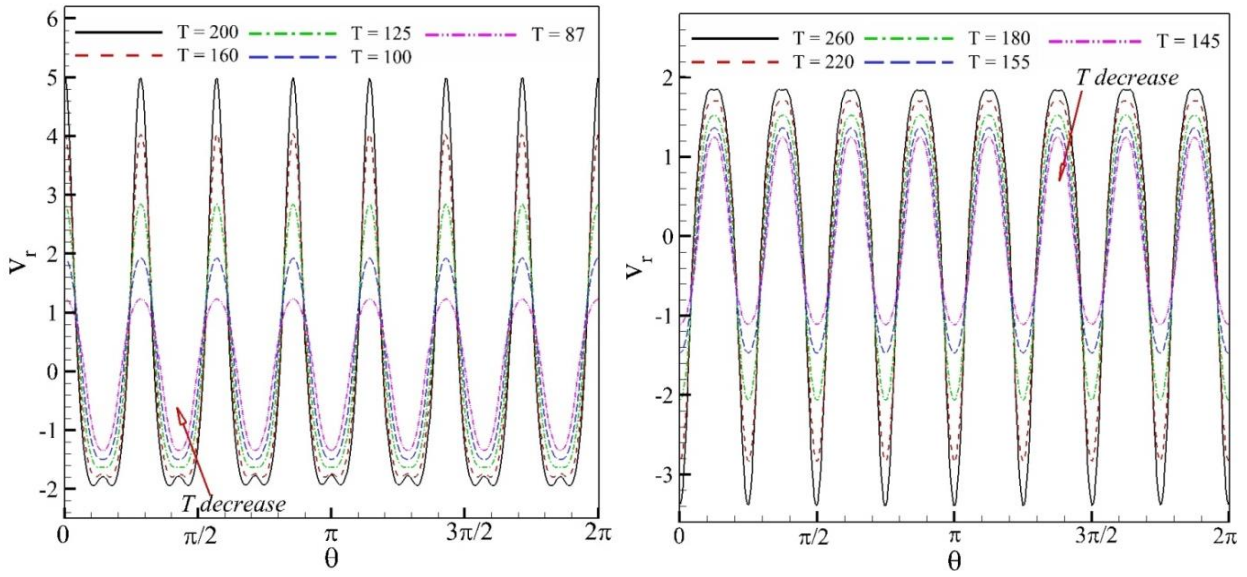

(a) (b)

FIG. 6. Radial velocity V_r at r = $(R_i+R_o)/2$ for different electric Rayleigh numbers, (a) inner and (b) outer injection.

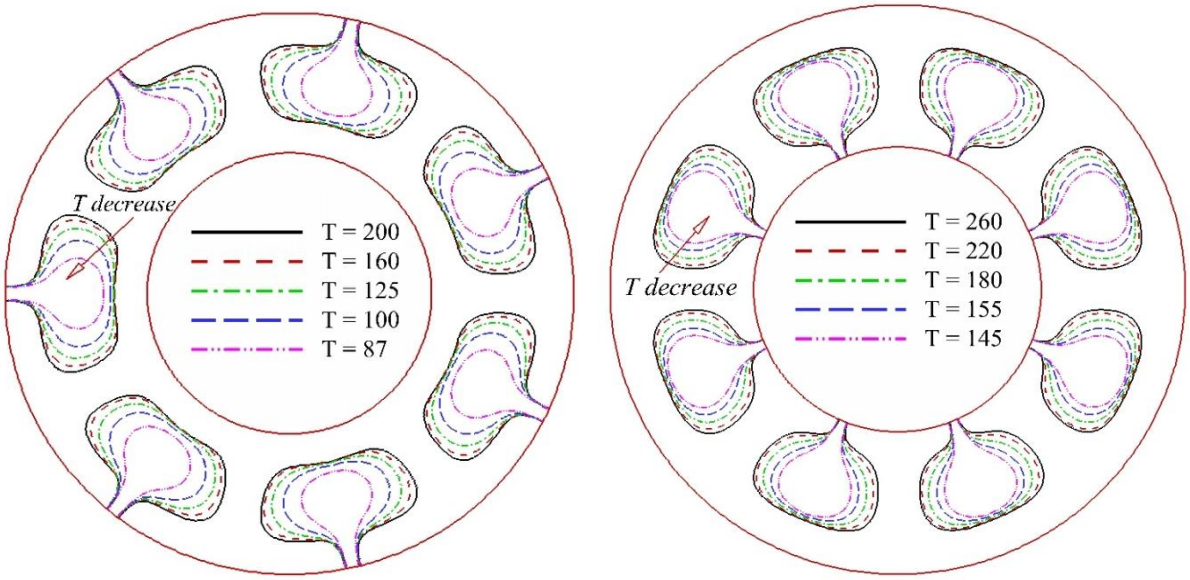

(a) (b)

FIG. 7. Variations of the region free of charges ($q < 0.05$) for different electric Rayleigh numbers T for (a) inner and (b) outer injection.

Along with the decrease of T, both V_r and the area of the charge-free region decreases, while the number of charge-free region remains the same. The area of the charge-free region is an

increasing function of the electric torque that drives the motion. The decrease of T results in the decrease of the torque and consequently the decrease of the area of the charge-free region [23]. At T smaller than T_{f1}, the small electric torque is unable to sustain the flow motion, and then the charge-free region suddenly disappears. Meanwhile the velocity amplitude jumps from a finite value to zero, which means the system returns back to the hydrostatic state. The nonlinear stability criteria for the inner and outer injection are found to be about 86.5 and 143.0, respectively. Figure 8 plots the hysteresis loops expressed by the electric Nusselt number Ne.

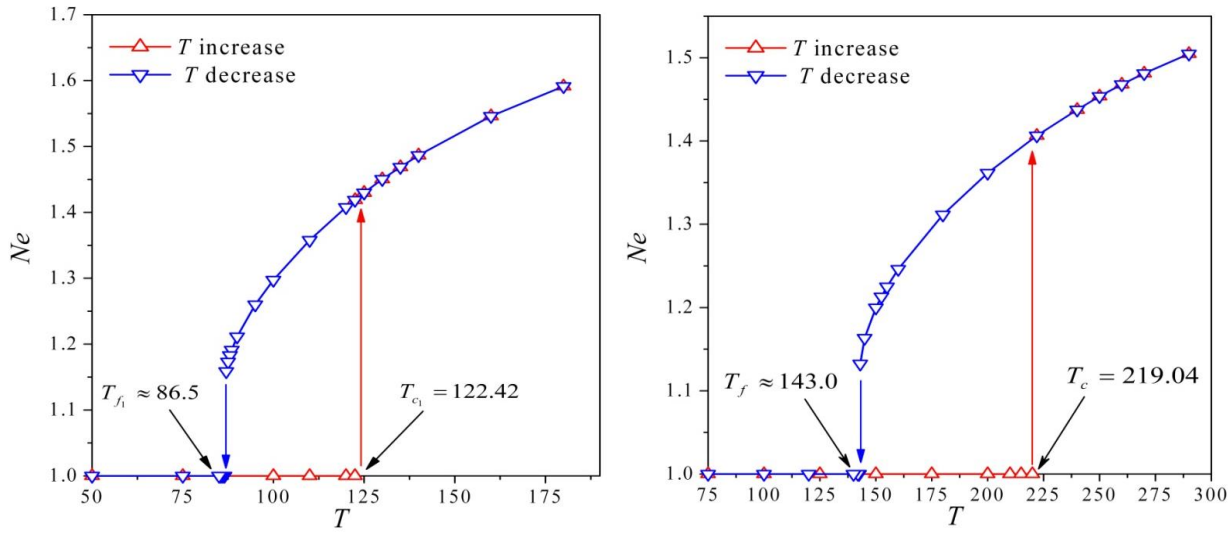

(a) (b)

FIG. 8. Hysteresis loops respresented by the electric Nusselt number Ne versus T for (a) inner and (b) outer injection.

In Table II we have summarized the values of T_c and T_{f1} obtained from our numerical simulations for different values of M. The linear stability analysis proved that T_c is independent of M. Our present numerical results have verified this point. It is shown that the maximum discrepancy between the analytical value of T_c and our numerical ones is less than 1%. Up today there is no nonlinear stability analysis in the annular geometry, and the relationship between T_{f1}

and M has not been theoretically investigated yet. However, our numerical results reveal that T_{f1} only weakly depends on M when M is small. For example, the nonlinear criterion is $T_{f1} = 141.0$ for $M = 5$ and $T_{f1} = 144.5$ for $M = 50, 100, 200$, showing a difference of 2.4%. This is the maximum difference we observed in all cases. It appears that the flow motion of $M \geq 20$ are viscous dominated and are close to the case of purely viscous case [32,37].

TABLE II. Dependence of the linear and nonlinear stability criteria on the mobility number M.

		Mobility number, M					
		5	10	20	50	100	200
Linear	Inner	122.56 (7)	122.42 (7)	122.40 (7)	122.73 (7)	122.61 (7)	122.55 (7)
	Outer	221.85(8)	219.04 (8)	219.02 (8)	220.63 (8)	220.43 (8)	221.05 (8)
Nonlinear	Inner	86.0	86.9	87.0	87.1	87.1	87.1
	Outer	141.0	143.3	144.0	144.5	144.5	144.5

Note: the analytical values of T_c (m_c) for the linear stability criterion is 122.54 (7) and 221.38 (8) for inner and outer injection, respectively. The numbers in parenthesis correspond to the number of vortex pairs observed numerically, and they are the same as m_c, the dominating Fourier mode.

4.4 A complete bifurcation diagram

We have explored the behavior of the system for higher values of T. The results for the inner injection case are summarized in figure 9. Starting from the fully developed flow at T=123.06, with 7 pairs of vortices, we increase the value of T. The electric Nusselt number Ne increases while keeping the structure of the flow. At $T \approx 205$ (point A in the figure) the system jumps to another steady state with 8 pairs of vortices (point B). Further increasing T to $T \approx 300$, the flow becomes oscillatory, and the flow pattern changes periodically between 8 and 9 pairs of vortices. If now we decrease T, the system does not jump back to the branch with 7 cells, but keeps the 8 cells structure until the electric torque is not strong enough to sustain the motion (point C). The

plots at the bottom of the figure show the flow structure and charge distribution for the three points. The critical value $T_{f2} \approx 88.5$ is slightly higher than T_{f1}, the value corresponding to the structure of 7 pairs of vortices. If this same procedure is applied to the outer injection case, the system keeps all the time the 8 cells pattern, up to $T \approx 350$, above which the flow becomes oscillatory, and 8 and 9 pairs of vortices alternatively appear. If the value of T is now decreased we recover the descending branch in figure 8b.

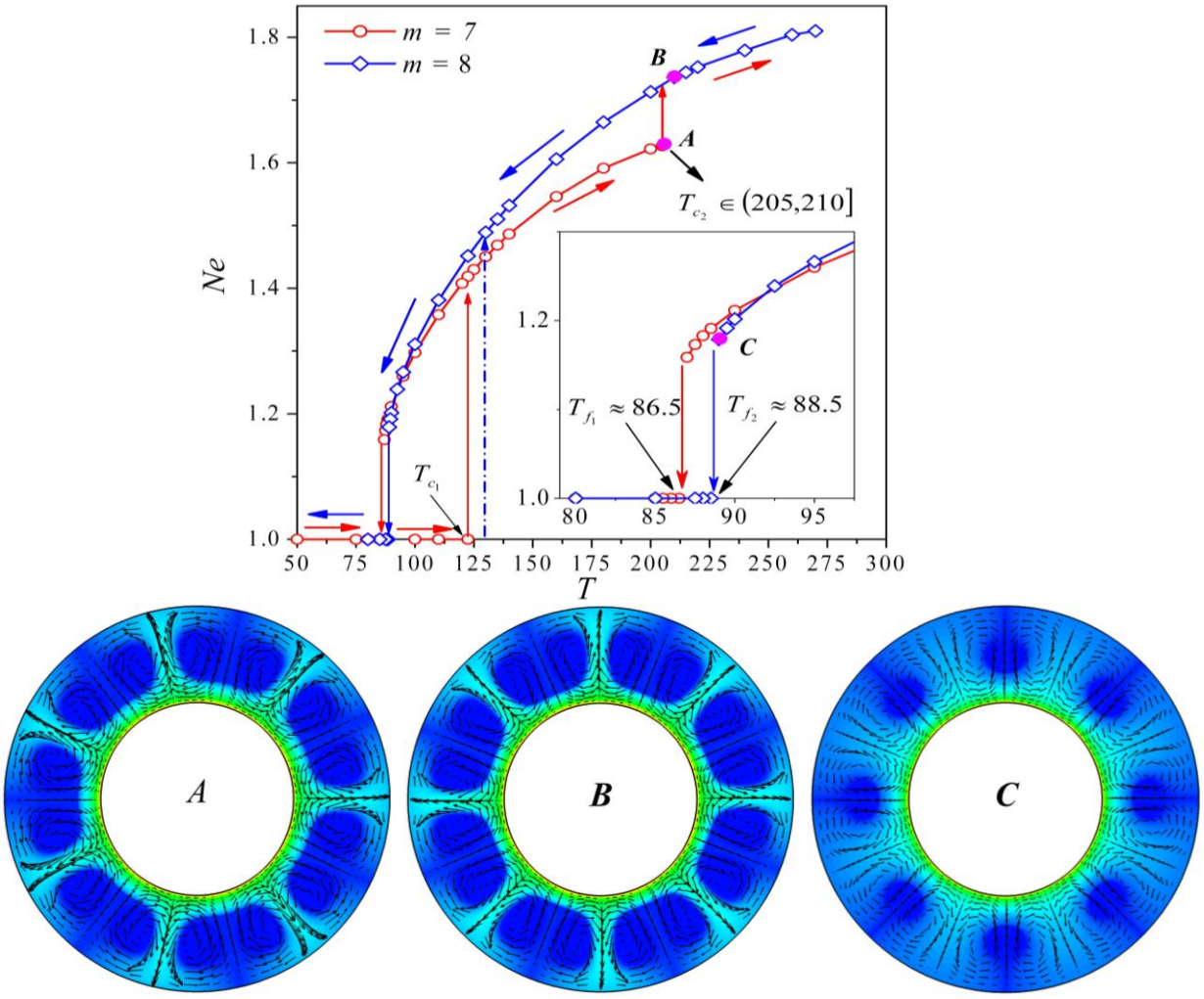

FIG.9. The complete bifurcation diagram for the inner injection case.

Previous numerical results in the planar configuration have shown the oscillatory flow pattern with varying numbers of vortices in the finite [29,31,33] and large [27,28,30] computational domains. In addition, a very similar phenomena have been observed in [38] with the cylindrical configuration. The difference lies in the critical values separating different states. Our values of T are always smaller than the ones presented in [38]. For example, with the inner injection case, the value of T separating the steady state of 8 pairs of vortices and the oscillatory state is higher than 500, much higher than the value we find (about 300). We attribute the discrepancy to the effect of physical and numerical diffusion embedded in the solutions of [38]. Generally the diffusion tends to stabilize the system and puts off the transition from steady to unsteady states [33,61]. On the one hand, the physical model used in [18,38] keeps the molecular diffusion term though with a small diffusion coefficient in the charge density equation. On the other hand, the uniform grid and the low order schemes used in [38] to solve the charge density equation inevitably introduce some numerical diffusion.

4.5 Modal analysis of the bifurcation

Figure 9 shows another way to reach the 8 cells branch (see the blue dashed line with upward arrow) in the inner injection case. Starting from the hydrostatic solution, we set the value of T at 132. Experimentally this can be achieved through a step voltage. In this case the the system jumps directly to the 8 cells branch. This new behavior has never been reported before and it can be explained with a simple modal analysis. Figure 10 shows the critical values for the modes with 6, 7, 8, and 9 cells as a function of Γ for the inner and outer injection cases. These curves are obtained from the 2D linear stability analysis. Table II gives the accurate numerical values. We

can see that the values corresponding to the 7 and 8 cells modes are very close in both cases. That means that just above the value of T_c both modes tend to be excited.

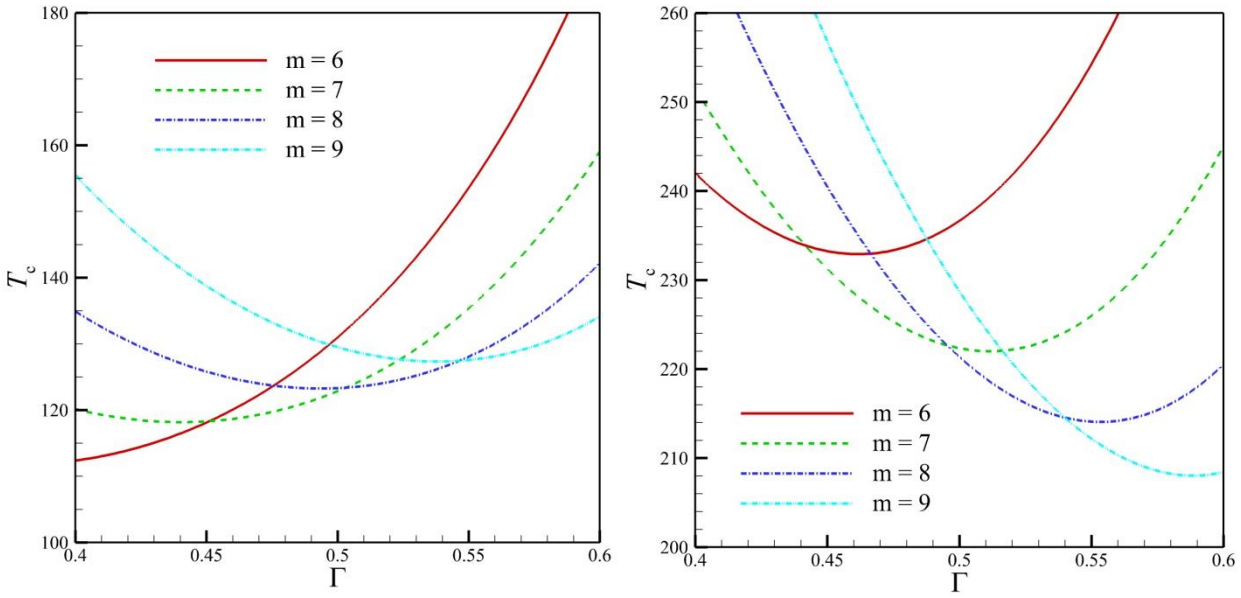

FIG. 10. Critical values of T for modes with 6, 7, 8 and 9 cells as a function of Γ for inner (a) and outer (b) injection.

TABLE II. The critical electric Rayleigh number T_c and dimensionless wave number m_c, $\Gamma = 0.5$.

Direction	Number of modes, m			
	m=6	m=7	m=8	m=9
Inner	130.961	122.844	123.306	129.503
outer	236.652	222.342	221.376	228.733

We have used a simple phenomenological modal analysis to understand the evolution of the modes. The velocity field can be expressed as a superposition of modes

$$\vec{u}(r,\theta,t) = \sum_m A_m(t)\vec{u}_m(r,\theta), \tag{13}$$

where r and θ are the cylindrical coordinates. The velocity field for each mode can be derived from the stream function

$$\psi_m(r,\theta) = B_m \sin(m\theta)(r-R_i)^2(r-R_o)^2, \tag{14}$$

the cylindrical components of the modal velocities being

$$u_{mr} = \frac{1}{r}\frac{\partial \psi_m}{\partial \theta}, \qquad u_{m\theta} = -\frac{\partial \psi_m}{\partial r} \tag{15}$$

The stream function is chosen so that the no slip boundary conditions on the inner and outer cylinders are fulfilled. Also, with this choice the modal velocities are orthogonal, that is, when integrating in the computational domain we have:

$$\int_\Omega \vec{u}_m \cdot \vec{u}_n dS = 0, \quad \text{if} \quad m \neq n. \tag{16}$$

The constant B_m is computed so that the maximum velocity of each modal velocity is 1.

The component $A_m(t_i)$ is computed at each time step by projecting the computed velocity field $\vec{u}(t_i)$,

$$A_m(t_i) = \frac{\int_\Omega \vec{u}(t_i) \cdot \vec{u}_m dS}{\int_\Omega \vec{u}_m \cdot \vec{u}_m dS}. \tag{17}$$

Figure 11 plots the time evolution of the modal components for the inner injection case and T=125 and T=150. We made these simulations using the top half cylinders with symmetric boundary conditions on the horizontal sides. The reason to do that is that the velocity field issued from the simulations with the complete domain is not necessarily aligned with the axis of figure 1. In the first case the system stays on the 7 cells branch and in the second one it jumps directly to the 8 cells branch. For T=125 the mode with m=7 becomes dominant, after a competition with the mode m=8. In the steady state the amplitudes of all the other modes are very small. For T=150 it is the mode m=8 which becomes dominant. In this case the amplitudes of the other modes are not as small as previously, and even the mode m=9 gets an amplitude greater than the mode m=7. Figure 11c plots the amplitudes for the modes m=7 and m=8 for T=300, showing the oscillation

between these two modes, as observed in the simulations for the whole domain. The other modes have also significant contributions in this case, but we have chosen to plot only two modes, for the sake of clarity.

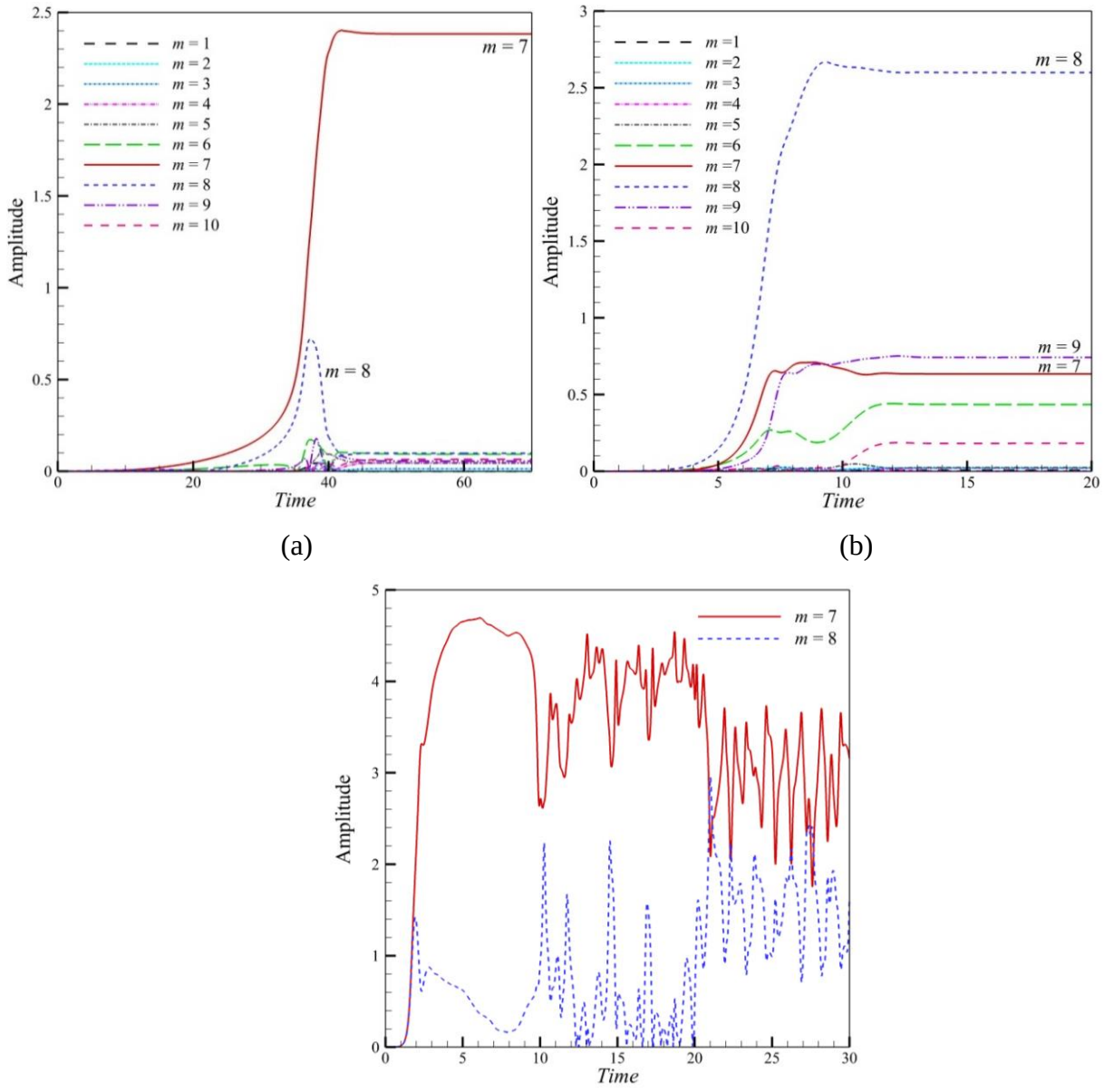

FIG. 11. Time evolution of the modal amplitudes for inner injection, (a) T=125, (b) T= 150 and (c) T=300.

For the outer injection case, following the same procedure, we have also tried different values of T ($>T_c$ = 221.38) in a wide range. However, up to T = 325, only one type of flow pattern showing 8 pairs of steady counter-rotating vortices (similar to Figure 5) is observed. Further tries with T > 325 lead to oscillatory flow patterns. This means that the mode of m=8 is always dominant in the range of $T \in [T_c, 325]$ for the outer injection case.

5. CONCLUSIONS

We have performed a theoretical and numerical analysis of the two-dimensional annular electroconvection induced by a strong unipolar injection of ions in a dielectric liquid contained between two coaxial cylinders. Compared to the problem of the planar configuration, two extra factors arise: the injection direction and the radius Γ. We consider a representative case with Γ = 0.5, and the injection can be either from the inner or outer cylinder. It is shown that for both injection directions the flow is characterized by the subcritical bifurcation, which means that there exist a linear stability criterion and a finite amplitude one corresponding to the onset and stop of the flow motion, respectively. The flow structure is characterized by a number of counter-rotating vortices and regions free of charges. We have determined the linear stability criteria expressed with the critical electric Rayleigh number T and the critical mode number from our direct numerical results and have compared them with the values predicted by the linear stability analysis. An excellent agreement is found. We have also extended the numerical study to higher values of T. For the inner injection, the system experiences a transition from a steady state with 7 pairs of vortices to another steady state with 8 pairs of vortices. Such a transition results in a new subcritical criterion, corresponding to the stop of the motion with 8 pairs of vortices. This behavior can be understood phenomenologically projecting the computed velocity field on a

simple modal expansion. As T increases the dominant mode changes, and eventually the flow oscillates between modes with 8 and 9 cells.

Till now there is no direct way to experimentally visualize the charge density distribution, the numerical results provided in this study may help gaining deeper insight of the electro-convective phenomena. In addition, the finite stability criteria we obtained numerically may serve as references for the coming weakly nonlinear stability analysis. This work may be extended in several interesting directions. In a future work, we will investigate the effects of the radius ratio on the linear and nonlinear stability criteria.

ACKNOWLEDGMENTS

This work was partially funded by the French Government program "Investissements d'Avenir" (LABEX INTERACTIFS, reference ANR-11-LABX-0017-01) (to Jian Wu), a grant of the French district Poitou- Charentes (to P. Traoré), and partially by financial support from the Spanish Ministerio de Cienciay Tecnología (MCYT) under Research Project No. FIS2011-25161 and Junta de Andalucía under research projects P10-FQM-5735 and P09-FQM-4584 (to A. T. Pérez).

REFERENCES

[1] A. Castellanos (Eds.), "Electrohydrodynamics", Springer, New York, 1998.

[2] P. J. Martin and A. T. Richardson, "Conductivity models of electrothermal convection in a plane layer of dielectric liquid", J. Heat Transfer, 106(1), 131-136 (1984).

[3] L. Onsager "Deviations from Ohm's law in weak electrolytes", J. Chem. Phys. 2(9), 599-615, (1934).

[4] J. C. Ryu, H. J. Park, J. K. Park and K. H. Kang, “New electrohydrodynamic flow caused by the Onsager effect”, Phys. Rev. Lett. 104(10), 104502, (2010).

[5] A. Denat, B. Gosse and J. P. Gosse, “Ion injections in hydrocarbons”, J. Electrostatics 7, 205-225, (1979).

[6] A. Alj, A. Denat, J. P. Gosse, B. Gosse and I. Nakamura, “Creation of charge carriers in nonpolar liquids”, IEEE Trans. Electr. Ins. 2, 221-231, (1985).

[7] J. M. Schneider and P. K. Watson, “Electrohydrodynamic stability of space-charge-limited currents in dielectric liquids. I. theoretical study,” Phys. Fluids 13(8), 1948-1954 (1970).

[8] J. M. Schneider and P. K. Watson, “Electrohydrodynamic stability of space charge limited currents in dielectric liquids: II. Experimental study”, Phys. Fluids 13(8), 1955-1961 (1970).

[9] A. Castellanos, “Coulomb-driven convection in Electrohydrodynamics,” IEEE Trans. Electr. Ins. 26(6), 1201-1215 (1991).

[10] P. Atten, “Electrohydrodynamic instability and motion induced by injected space charge in insulating liquids,” IEEE Trans. Electr. Ins. 3(1), 1-17 (1996).

[11] Y. K. Suh, “Modeling and simulation of ion transport in dielectric liquids-Fundamentals and review,” IEEE Trans. Electr. Ins., 19(3), 831-848 (2012).

[12] P. Atten and R. Moreau, "Stabilité électrohydrodynamique des Liquides Isolants Soumis à Une Injection Unipolaire," J. Mécanique 11(3), 471-521 (1972).

[13] J. C. Lacroix, P. Atten, E. J. Hopfinger, “Electroconvection in a dielectric layer subjected to unipolar injection,” J. Fluid Mech. 69, 539-563 (1975).

[14] X. Zhang, “Electro-optic signatures of turbulent electroconvection in dielectric liquids”, Appl. Phys. Lett. 104(20), 202901 (2014).

[15] A. T. Richardson and R. Poulter, “Electrophoretic instability in a diffusion-free dielectric liquid in an annular geometry,” J. Phys. D: Appl. Phys. 9(4), L45 (1976).

[16] A. T. Richardson, “The linear instability of a dielectric liquid contained in a cylindrical annulus and subjected to unipolar charge injection,” Q. J. Mech. Appl. Math. 33(3), 277-292 (1980).

[17] N. Agrät and A. Castellanos, “Linear convective patterns in cylindrical geometry for unipolar injection,” Phys. Fluids 2(1), 37-44 (1990).

[18] D. V. Fernandes, H. D. Lee, S. Park, and Y. K. Suh, “Electrohydrodynamic instability of dielectric liquid between concentric circular cylinders subjected to unipolar charge injection,” J. Mech. Sci. Tech. 27(2), 461-467 (2013).

[19] S. Oliveri and P. Atten, “The linear stability of a spherical liquid layer subjected to a unipolar charge injection,” Phys. Fluids 29(5), 1378-1385 (1986).

[20] F. Pontiga and A. Castellanos, “A dissociation-injection model for non-polar liquid conduction and wire-cylinder geometry,” IEEE Trans. Electr. Ins. 4(2), 224-237 (1997).

[21] N. Felici, “Phénomènes hydro et aérodynamiques dans la conduction des diélectriques fluides,” Revue Générale de l’Electricité 78, 717-734 (1969).

[22] P. Atten and J. C. Lacroix, “Non-linear hydrodynamic stability of liquids subjected to unipolar injection,” J. Mécanique 18, 469-510 (1979).

[23] A. Castellanos, P. Atten, and A. T. Pérez, “Finite amplitude electroconvection in liquid in the case of weak unipolar injection,” CH PhysicoChemical Hydrodynamics 9 (3/4), 443-452 (1987).

[24] P. Atten and J. C. Lacroix,"Electrohydrodynamic stability of liquids subjected to unipolar injection: non linear phenomena", J. Electrost. 5, 439-452 (1978).

[25] R. Chicón, A. Castellanos, and E. Martín, "Numerical modelling of Coulomb-driven convection in insulating liquids", J. Fluid Mech. 344, 43-66 (1997).

[26] P. A. Vázquez, G. E. Georghiou and A. Castellanos A, "Characterization of injection instabilities in electrohydrodynamics by numerical modelling: comparison of particle in cell and flux corrected transport methods for electroconvection between two plates", J. Phys. D: Appl. Phys. 39, 2754-2763 (2006).

[27] Cerizza D, "Electroconvection in three dimensions: a numerical study", Master Thesis, Politecnico di Milano, Italy, 2007.

[28] P. A. Vázquez, G. E. Georghiou, and A. Castellanos, "Numerical analysis of the stability of the electrohydrodynamic (EHD) electroconvection between two plates", J. Phys. D: Appl. Phys. 41, 175303-175313 (2008).

[29] P. Traoré and A. T. Pérez, "Two-dimensional numerical analysis of electroconvection in a dielectric liquid subjected to strong unipolar injection," Phys. Fluid, 24(3), 037102 (2012).

[30] A. Kourmatzis and J. S. Shrimpton, "Turbulent three-dimensional dielectric electro-hydrodynamic convection between two plates," J. Fluid Mech. 696, 228-262 (2012).

[31] P. A. Vázquez and A. Castellanos, "Numerical simulation of EHD flows using Discontinuous Galerkin Finite Element methods", Comput. Fluids 84, 270-278 (2013).

[32] P. Traoré and J. Wu, "On the limitation of imposed velocity field strategy for Coulomb-driven electroconvection flow simulations," J. Fluid Mech. 727, R3 (2013).

[33] J. Wu, P. Traoré, T. Fang-Bao, A. T. Pérez, C. Louste and L. Dascalescu , "Effect of mobility parameter on the oscillatory electro-convection of dielectric liquids subject to strong unipolar charge injection," IEEE Trans. Ind. Appl. DOI 10.1109/TLA.2014.2301872, to appear.

[34] P.L. Roe, "Characteristic-based schemes for the Euler equations," Ann. Rev. Fluid Mech. 18(1), 337-365(1986).

[35] R. J. LeVeque, "Finite volume methods for hyperbolic problems," Cambridge university press (2002).

[36] K. Adamiak, "Numerical models in simulating wire-plate electrostatic precipitators: a review," J. Electrost. 71, 637-680 (2013).

[37] A. Castellanos and P. Atten, "Numerical modeling of finite amplitude convection of liquids subjected to unipolar injection," IEEE Trans. Ind. Appl. IA-23, 825-830 (1987).

[38] D. V. Fernandes, H. D. Lee, S. Park, and Y. K. Suh, "Numerical simulation of the electro-convective onset and complex flows of dielectric liquid in an annulus," J. Mech. Sci. Tech. 26(12), 3785-3793 (2012).

[39] M. Takashima, "Electrohydrodynamic instability in a dielectric fluid between two coaxial cylinders", Q. J. Mech. Appl. Math. 33(1), 93-103 (1980).

[40] L. Yang, S. M. Gubanski, Y. V. Serdyuk, J. Schiessling, "Dielectric properties of transformer oils for HVDC applications," IEEE Trans. Electr. Ins. 19(6), 1926-1933 (2012).

[41] M. S. Zadeh, "Measurement of ion mobility in dielectric liquids," M.S. thesis, Chalmers University of Technology (2011).

[42] J. Fernández and R. Poulter, "Radial mass flow in electrohydrodynamically-enhanced forced heat transfer in tubes," Int. J. Heat Mass Transfer, 30(10), 2125-2136 (1987).

[43] J. Cotton, A. J. Robinson, M. Shoukri, and J. S. Chang, "A two-phase flow pattern map for annular channels under a DC applied voltage and the application to electrohydrodynamic convective boiling analysis," Int. J. Heat Mass Transfer 48, 5563-5579 (2005).

[44] J. L. Fernandez, "Electrohydrodynamic enhancement of forced convection heat transfer in tubes," Ph.D. thesis, University of Bristol (1975).

[45] P. Atten and L. Elouadie, "EHD convection in a dielectric liquid subjected to unipolar injection: coaxial wire/cylinder geometry," J. Electrostatics 34(2), 279-297 (1995).

[46] A.T. Pérez, P. Atten, B. Malraison, L. Elouadie, and F. M. J. McCluskey, "Heat transfer augmentation induced by electrically generated convection in liquid," In: R. K. Shah, E. N. Ganic and K. T. Yang (Eds.), Exp. Heat Transfer, Fluid Mech. and Thermodynamics, Elsevier, Amsterdam, 941-947 (1988).

[47] A. T. Pérez and A. Castellanos, "Role of charge diffusion in finite-amplitude electro-convection", Phys. Rev. A 40(10), 5844 (1989).

[48] R. Tobazéon, "Electrohydrodynamic instabilities and electroconvection in the transient and AC regime of unipolar injection in insulating liquids: A review," J. Electrostatics, 15(3), 359-384 (1984).

[49] J. H. Ferziger and M. Perić, "Computational methods for fluid dynamics," Berlin: Springer, 2002.

[50] P. Traoré, Y. M. Ahipo, and C. Louste, "A robust and efficient finite volume scheme for the discretization of diffusive flux on extremely skewed meshes in complex geometries," J. Comput. Phys. 228(14), 5148-5159 (2009).

[51] S. V. Patankar and D. B. Spalding, “A calculation procedure for heat, mass and momentum transfer in three-dimensional parabolic flows,” Int. J. Heat Mass Transfer, 15(10), 1787-1806, (1972).

[52] J. Wu, P. Traoré, and C. Louste, “An efficient finite volume method for electric field-space charge coupled problems,” J. Electrostatics 71(3), 319-325 (2013).

[53] R. J. LeVeque, “High-resolution conservative algorithms for advection in incompressible flow”. SIAM J. Numer. Anal. 33(2), 627-665 (1996).

[54] P. K. Sweby, “High resolution schemes using flux limiters for hyperbolic conservation laws”, SIAM J. Numer. Anal. 21(5), 995-1011 (1984).

[55] P. H. Gaskell and A. K. C. Lau, “Curvature-compensated convective transport: SMART, A new boundedness-preserving transport algorithm,” Int. J. Numer. Meth. Fluids 8(6), 617-641 (1988).

[56] D. J. Mavriplis, “Revisiting the least-squares procedure for gradient reconstruction on unstructured meshes,” AIAA paper 2003-3986, (2003).

[57] B. Malraison and P. Atten , “Chaotic behavior of instability due to unipolar ion injection in a dielectric liquid,” Phys. Rev. Lett. 49, 723-726 (1982).

[58] J. Kierzenka and Shampine LF. “A BVP Solver Based on Residual Control and the MATLAB PSE”, ACM Trans. Math. Software 27(3), 299-316, (2001).

[59] P. Tsai, Z. A. Daya, V. B. Deyirmenjian and S. W Morris, “Direct numerical simulation of supercritical annular electroconvection,” Phys. Rev. E 76(2), 026305 (2007).

[60] N. Felici, “Phénomènes hydro et aérodynamiques dans la conduction des diélectriques fluids”, Revue Générale de l’Electricité 78, 717-734 (1969).

[61] T. Tagawa and H. Ozoe, “Effect of prandtl number and computational schemes on the oscillatory natural convection in an enclosure”, Numer. Heat Transfer. Part A 30 (3), 271-282, (1996).